A Subgridding Scheme Based on the FDTD Method and HIE-FDTD Method

Juan Chen and Anxue Zhang

School of Electronic and Information Engineering
Xi'an Jiaotong University, Xi'an 710049, China
anxuezhang@mail.xjtu.edu.cn

Abstract- To reduce the computer memory and time of the finite-difference time-domain (FDTD) method when the problems are simulated with fine structural features, the subgridding scheme that applies higher resolution only around critical areas is often used. In this paper, a new subgridding scheme is proposed which is based on the hybrid implicit-explicit finite-difference time-domain (HIE-FDTD) method and FDTD algorithm. The field components in fine local grids are updated using the HIE-FDTD method, and in the coarse main grids conventional FDTD method is utilized. Due to the weakly conditional stability of the HIE-FDTD method, the technique achieves the same time marching step in the whole domain as employed in the coarse FDTD scheme, and the need for the temporal interpolation of the fields in the fine grids is obviated, hence, the hybrid HIE-FDTD subgridding scheme is less time consuming and easy to implement. Practical application of hybrid algorithm in the simulation of the shielding effectiveness of an enclosure is reported.

Index Terms- FDTD method, HIE-FDTD method, subgridding scheme, weakly conditional stability.

I. INTRODUCTION

The finite-difference time-domain (FDTD) method [1] has been proven to be an effective means that provides accurate predictions of field behaviors for varieties of electromagnetic interaction problems. When there exists a fine structural feature compared with other parts in the computational domain, the intuitive approach is to discretize the whole computational domain with a very fine spatial increment in order to achieve enough spatial resolution. This will lead to excessive use of computation resources including computer memory and CPU time.

To circumvent this problem, the subgridding method for local mesh refinement is proposed as an efficient tool to enhance the FDTD algorithm [2-7].The subgridding method uses a fine mesh only in the geometrically critical or electrically small areas and a coarse mesh elsewhere. Inside the fine grid region, the temporal step size must be adjusted to a smaller value in order to meet the stability criterion. Therefore, to synchronize the timing between the two regions, many time steps need to be executed in the fine grid region within a time step of the coarse grid region.

A novel subgridding scheme using the hybrid implicit-explicit finite-difference time-domain (HIE-FDTD) method [8-12] to process the fine grid region is proposed in this article. The HIE-FDTD method is weakly conditionally stable, such the step size in the fine grid region can be set equal to that in the coarse grid region to speed up the computation. Temporal interpolation at the fine and coarse grids interface is no longer necessary. Accuracy of the proposed approach is verified by comparing with FDTD method and HIE-FDTD using a fine spatial increment for the total computational domain, and the memory requirements of all these methods are compared. Practical application of the hybrid subgridding algorithm in the simulation of the shielding effectiveness of an enclosure is reported.

II. THEORY

A. HIE-FDTD method

Without loss of generality, assume that the fine mesh is along the z-direction. Figure 1 shows the interface between the fine and coarse grid regions and the corresponding field components in each region. The ratio between spatial increments in the two regions is denoted by $m = \Delta Z / \Delta Z_f$, where Δz and Δz_f are the spatial increments along the

z-axis in the coarse grid region, and in the fine grid region, respectively. The ratio m is set to 3 as an illustrating example in Figure 1. E_z, E_x, and H_y represent field components in the coarse grid region, and E_{zf}, E_{xf}, and H_{yf} represent field components in the fine grid region.

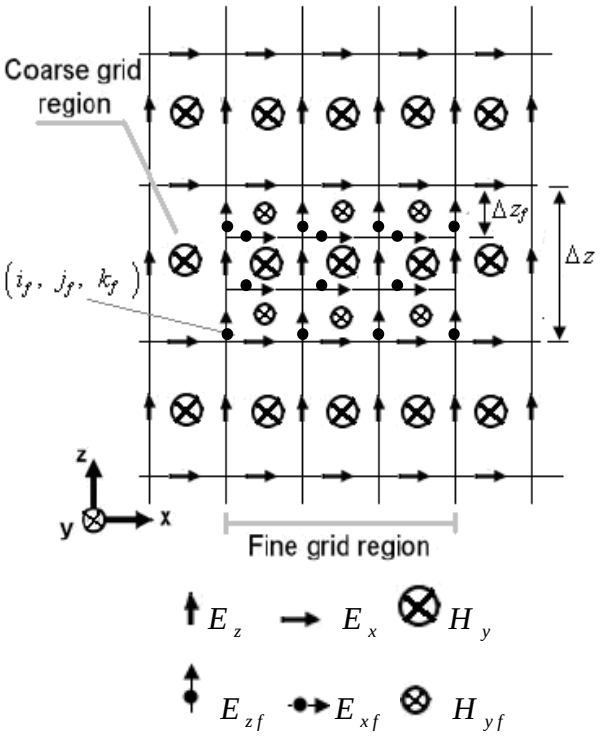

Fig. 1. The field components around the fine and coarse grid interface.

The HIE-FDTD scheme is employed in the fine grid region to update the field components where n and Δt are the index and size of time-step, Δx and Δy are the spatial increments respectively in x- and y-directions, ε and μ are the permittivity and permeability of the surrounding media, respectively. The E_{xf} and H_{yf} components in the HIE-FDTD method are expressed in equations (1) and (2).

Updating of the E_{xf} component, as shown in eq. (1), needs the unknown H_{yf} component at the same time, thus the E_{xf} component has to be updated implicitly. By substituting (2) into (1), the equation for E_{xf} field can be represented by equation (3).

$$
\begin{aligned}
E_{xf}^{n+1}\left(i+\frac{1}{2},j,k\right) &= E_{xf}^{n}\left(i+\frac{1}{2},j,k\right) \\
&+\frac{\Delta t}{\varepsilon\Delta y}H_{zf}^{n+\frac{1}{2}}\left(i+\frac{1}{2},j+\frac{1}{2},k\right) \\
&-\frac{\Delta t}{\varepsilon\Delta y}H_{zf}^{n+\frac{1}{2}}\left(i+\frac{1}{2},j-\frac{1}{2},k\right) \\
&-\frac{\Delta t}{2\varepsilon\Delta z_f}H_{yf}^{n+1}\left(i+\frac{1}{2},j,k+\frac{1}{2}\right) \\
&+\frac{\Delta t}{2\varepsilon\Delta z_f}H_{yf}^{n+1}\left(i+\frac{1}{2},j,k-\frac{1}{2}\right) \\
&-\frac{\Delta t}{2\varepsilon\Delta z_f}H_{yf}^{n}\left(i+\frac{1}{2},j,k+\frac{1}{2}\right) \\
&+\frac{\Delta t}{2\varepsilon\Delta z_f}H_{yf}^{n}\left(i+\frac{1}{2},j,k-\frac{1}{2}\right), \qquad (1)
\end{aligned}
$$

$$
\begin{aligned}
H_{yf}^{n+1}\left(i+\frac{1}{2},j,k+\frac{1}{2}\right) &= H_{yf}^{n}\left(i+\frac{1}{2},j,k+\frac{1}{2}\right) \\
&+E_{zf}^{n+\frac{1}{2}}\left(i+1,\ j,k+\frac{1}{2}\right) \\
&-\frac{\Delta t}{\mu\Delta x}E_{zf}^{n+\frac{1}{2}}\left(i,\ j,k+\frac{1}{2}\right) \\
&-\frac{\Delta t}{2\mu\Delta z_f}E_{xf}^{n+1}\left(i+\frac{1}{2},\ j,k+1\right) \\
&+\frac{\Delta t}{2\mu\Delta z_f}E_{xf}^{n+1}\left(i+\frac{1}{2},\ j,k\right) \\
&-\frac{\Delta t}{2\mu\Delta z_f}E_{xf}^{n}\left(i+\frac{1}{2},\ j,k+1\right) \\
&+\frac{\Delta t}{2\mu\Delta z_f}E_{xf}^{n}\left(i+\frac{1}{2},\ j,k\right), \qquad (2)
\end{aligned}
$$

$$
\left[1+2s_1\right]E_{xf}^{n+1}\left(i+\frac{1}{2},j,k\right)
$$

$$
\begin{aligned}
&-s_1\left[E_{xf}^{n+1}(i+\frac{1}{2},j,k+1)+E_{xf}^{n+1}(i+\frac{1}{2},j,k-1)\right]\\
&=E_{xf}^{n}\left(i+\frac{1}{2},j,k\right)+\frac{\Delta t}{\varepsilon\Delta z_f}H_{yf}^{n}\left(i+\frac{1}{2},j,k+\frac{1}{2}\right)\\
&-\frac{\Delta t}{\varepsilon\Delta z_f}H_{yf}^{n}\left(i+\frac{1}{2},j,k-\frac{1}{2}\right)\\
&-s_2\begin{bmatrix}E_{zf}^{n+\frac{1}{2}}\left(i+1,j,k+\frac{1}{2}\right)-E_{zf}^{n+\frac{1}{2}}\left(i,j,k+\frac{1}{2}\right)\\-E_{zf}^{n+\frac{1}{2}}\left(i+1,j,k-\frac{1}{2}\right)+E_{zf}^{n+\frac{1}{2}}\left(i,j,k-\frac{1}{2}\right)\end{bmatrix}\\
&+s_1\begin{bmatrix}E_{xf}^{n}\left(i+\frac{1}{2},j,k+1\right)-2E_{xf}^{n}\left(i+\frac{1}{2},j,k\right)\\+E_{xf}^{n}\left(i+\frac{1}{2},j,k-1\right)\end{bmatrix}\\
&-\frac{\Delta t}{\varepsilon\Delta y}\begin{bmatrix}H_{zf}^{n+\frac{1}{2}}\left(i+\frac{1}{2},j+\frac{1}{2},k\right)\\-H_{zf}^{n+\frac{1}{2}}\left(i+\frac{1}{2},j-\frac{1}{2},k\right)\end{bmatrix},
\end{aligned}
\tag{3}
$$

where, $s_1=\dfrac{\Delta t^2}{4\varepsilon\mu\Delta z_f{}^2}, s_2=\dfrac{\Delta t^2}{2\mu\varepsilon\Delta x\Delta z_f}$.

The HIE-FDTD method is weakly conditionally stable. The time step size in the HIE-FDTD method is determined as follows:

$$\Delta t \le 1\Big/\left(c\sqrt{\left(1/\Delta x\right)^2+\left(1/\Delta y\right)^2}\right), \tag{4}$$

here, c is the light velocity in the medium.

In the coarse grid region, field components are updated using Yee's FDTD expressions, thus, in the whole domain, the time step size can be set as that in the FDTD scheme, namely,

$$\Delta t \le 1\Big/\left(c\sqrt{\left(1/\Delta x\right)^2+\left(1/\Delta y\right)^2+\left(1/\Delta z\right)^2}\right).$$

Temporal synchronization is then easily achieved, and only spatial interpolation is needed to be taken care of at the interface.

B. Spatial interpolation at the interface

Field components in the fine and coarse grid regions are updated using different schemes. For nodes located near the fine and coarse grid interface, proper care must be taken in order to avoid the discontinuity in fields which will lead to instability of the computation. Suppose the interface is set at $i=i_f$, $j=j_f$, and $k=k_f$, as shown in Figure 1.

In Figure 1, the coarse and fine grid ratio *m* is equal to 3. At the interface $j=j_f$, electric field $E_z\left(i_f+n,j_f,k_f+\frac{1}{2}\right)$ ($0\le n\le 3$)is obtained from E_{zf} at each time step through a simple interpolation as:

$$
\begin{aligned}
&E_z\left(i_f+n,j_f,k_f+\frac{1}{2}\right)\\
&=\frac{\sum_{m=0}^{2}E_{zf}\left(i_f+n,j_f,k_f+m+\frac{1}{2}\right)\Delta z_f\left(k_f+m\right)}{\sum_{m=0}^{2}\Delta z_f\left(k_f+m\right)}\\
&\left(0\le n\le 3\right).
\end{aligned}
\tag{5}
$$

The E_{zf} components at the interfaces $i=i_f$ and $j=j_f$ are calculated as follows:

$$
\begin{aligned}
&E_{zf}^{n+1}\left(i_f,j_f,k_f+m+\frac{1}{2}\right)\\
&=E_{zf}^{n}\left(i_f,j_f,k_f+m+\frac{1}{2}\right)\\
&+\frac{\Delta t}{\varepsilon\Delta x}H_{yf}^{n}\left(i_f+\frac{1}{2},j_f,k_f+m+\frac{1}{2}\right)
\end{aligned}
$$

$$-\frac{\Delta t}{\varepsilon \Delta x} H_y^n\left(i_f-\frac{1}{2}, j_f, k_f+\frac{1}{2}\right)$$
$$-\frac{\Delta t}{\varepsilon \Delta y} H_{xf}^n\left(i_f, j_f+\frac{1}{2}, k_f+m+\frac{1}{2}\right)$$
$$+\frac{\Delta t}{\varepsilon \Delta y} H_x^n\left(i_f, j_f-\frac{1}{2}, k_f+\frac{1}{2}\right)$$
$$\left(0 \le m \le 2\right). \tag{6}$$

Similarly, at the interface $j = j_f$, the magnetic field $H_y\left(i_f+n+\frac{1}{2}, j_f, k_f+\frac{1}{2}\right)$ $(0 \le n \le 2)$ is obtained from H_{yf} at each time step as:

$$H_y\left(i_f+n+\frac{1}{2}, j_f, k_f+\frac{1}{2}\right)$$
$$=\frac{\sum_{m=0}^{2} H_{yf}\left(i_f+n+\frac{1}{2}, j_f, k_f+m+\frac{1}{2}\right)\Delta z_f\left(k_f+m\right)}{\sum_{m=0}^{2}\Delta z_f\left(k_f+m\right)}$$
$$\left(0 \le n \le 2\right). \tag{7}$$

The H_{yf} components are updated by using eq. (2).

The flowchart of the algorithm procedure is shown in Figure 2.

It should be noted that, the scheme above is only suitable to the question with fine mesh along z-direction. If the fine mesh is along y (or/and x)-direction, the scheme can be derived by following the same analysis.

III. SIMULATION RESULTS

To demonstrate the accuracy and efficiency of the proposed subgridding method, a simulation of the shielding effectiveness of an enclosure is employed. The geometric configuration of the enclosure is shown in Figure 3. The length, width, and height of the enclosure are 30 cm, 30 cm, and 12 cm, respectively. A thin slot is cut on the front side of the enclosure. The length and width of the slot are 20 cm and 3 cm. A uniform plane electromagnetic wave, polarized in the $\hat{z}$ direction and traveling along the $\hat{y}$ direction, incident on the aperture. The time dependence of the excitation function is as follows,

$$E_{in}^z(t) = \exp[-\alpha(t-t_0)^2], \tag{8}$$

where α and t_0 are constants. Here, we choose $\alpha = 0.31\times 10^{19}$ s^{-2}, and $t_0 = 2.0\times 10^{-9}$ s. In such a case, the highest frequency of interest is 1 GHz.

To model the slot precisely, a fine mesh must be utilized in the region around the slot, as shown in Figure 4. Here, we choose $\Delta x = \Delta y = 3$ cm., $\Delta z = 2.25$cm, $\Delta z_f = 0.6$cm. To satisfy the stability condition of the FDTD algorithm, the time-step size for the FDTD in the fine grid region is $\Delta t \le 19.24$ ps. To improve the computation efficiency, we utilize the HIE-FDTD method in the fine grid region, thus, the step size in the fine grid region can be set equal to that in the coarse grid region, that is, $\Delta t = 51.45$ ps. Six perfectly matched layers are used to terminate all six sides of the lattice.

Applying the new subgridding scheme to compute the electric field component E_z and the shielding effectiveness (SE) at the central point of the enclosure, the results are shown in Figures 5 and 6. For the sake of comparison, we also present the results at the same position obtained by using the FDTD method and the HIE-FDTD method, respectively. In the FDTD method and the HIE-FDTD method, only the fine space increment is used. The time step sizes in the FDTD, HIE-FDTD, and sungridding schemes are 19.24 ps, 70.71 ps, and 51.45 ps, respectively. It can be seen from Figures 5 and 6 that, the results calculated by using these three methods agree well with each other, which shows that the subgidding scheme has high accuracy.

The computation time and the memory requirements of the FDTD, HIE-FDTD, and subgridding scheme in this simulation are shown in Table 1. Apparently, the proposed subgridding scheme consumes less computer memory and much less computation time compared to the conventional FDTD method and HIE-FDTD method which discretize the whole computation domain with a fine grid.

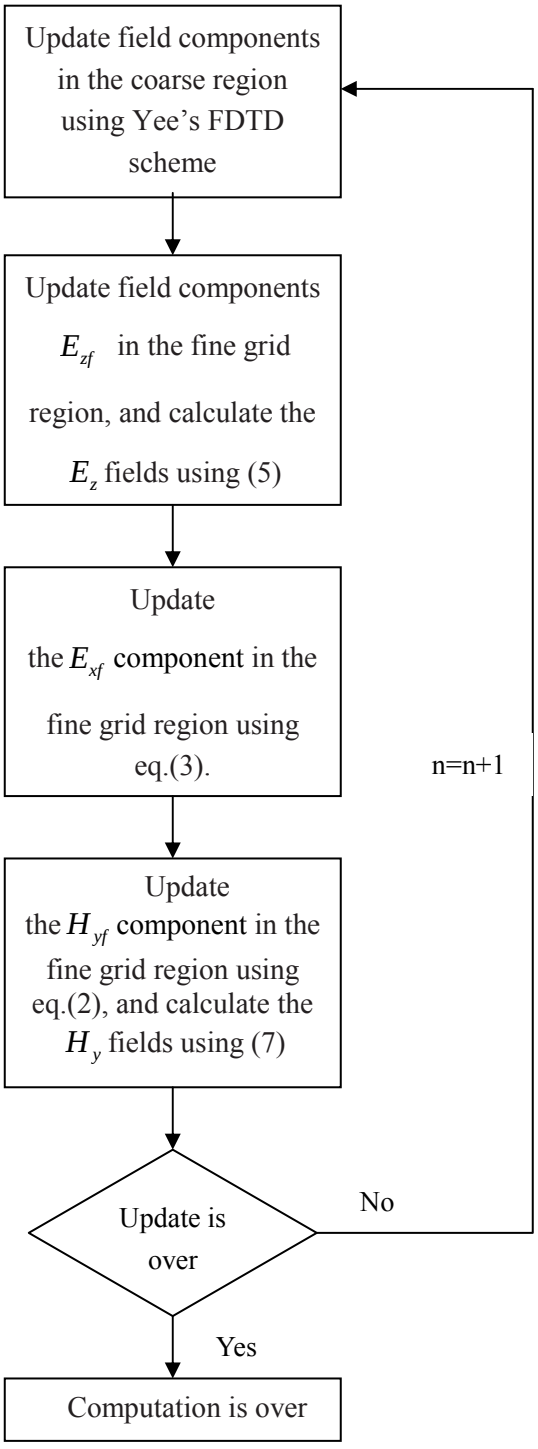

Fig. 2. The flowchart of the subgridding scheme.

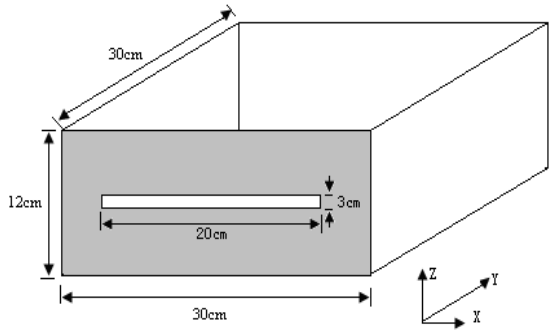

Fig. 3. Geometric configuration of the numerical simulation.

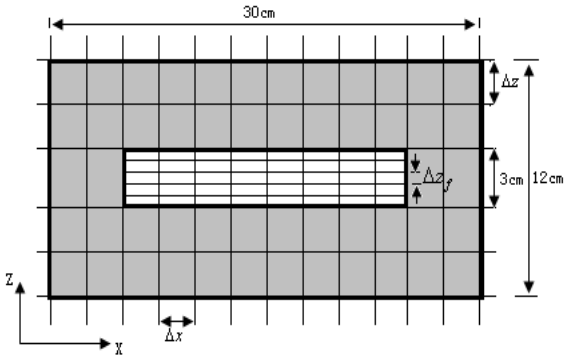

Fig. 4. Spatial increments of the front side of the enclosure.

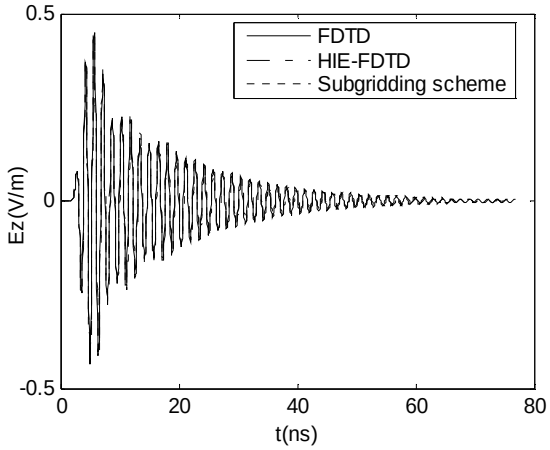

Fig. 5. Comparison of E_z component calculated by different methods.

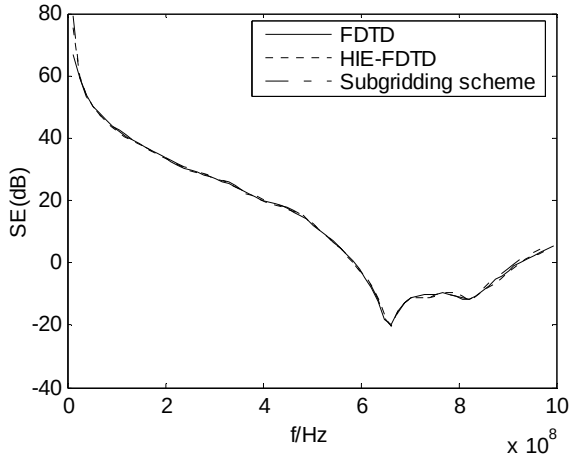

Fig. 6. Comparison of SE calculated by different methods.

Table 1: The computation time and the memory requirements of three methods

Sample	FDTD	HIE-FDTD	Subgridding Scheme
time (s)	1072.92	647.74	353.47
Memory (Mb)	16.85	18.30	15.14

To demonstrate the accuracy of the proposed subgridding method further, the relationship between the relative error and the grid size ratio *m* is shown in Figure 7. For the sake of comparison, the relative error of hybrid alternating direction implicit (ADI)-FDTD subgridding scheme [5] is also shown in this figure. Relative error is defined as,

$$err(\%) = \frac{\sum_{t=0}^{T} \left| E_z^{'}(t) - E_z(t) \right|}{T}, \qquad (9)$$

here, $E_z^{'}(t)$ is the result calculated by the proposed subgridding method or hybrid ADI-FDTD subgridding scheme; $E_z(t)$ is the result calculated by the FDTD method; T is the total time steps.

It can be seen from Figure 7 that, as the increase of the ratio *m*, the errors both of the proposed subgridding method and the hybrid ADI-FDTD subgridding scheme are decreased, and the accuracy of the proposed subgridding method is higher than that of hybrid ADI-FDTD

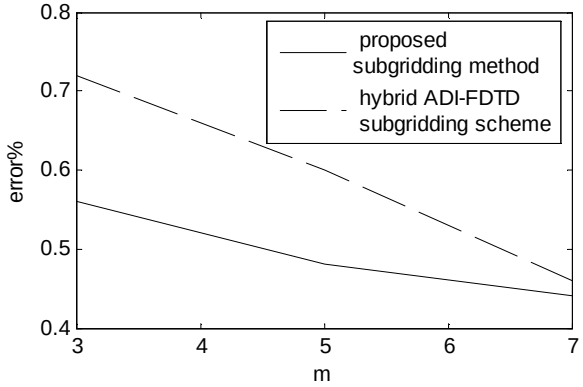

Fig. 7. The relationship between the error and the grid size ratio.

subgridding scheme. It is due to that the accuracy of HIE-FDTD method is over the ADI-FDTD method [9].

IV. CONCLUSION

A novel subgridding scheme combining the HIE-FDTD method and the conventional FDTD method is presented. The HIE-FDTD scheme is used for the subgridding regions and the FDTD scheme is employed for the coarse grid regions. With the weakly conditional stability of the HIE-FDTD algorithm, the subgridding scheme achieves the same time-step size in the entire computational domain. Hence, this technique is very simple to implement and saves considerable simulation time. The hybrid HIE-FDTD subgridding scheme can be used to all those cases where the conventional subgridding FDTD method is applicable, but with less computer memory and much less computation time.

ACKNOWLEDGMENT

This work was supported by the National Natural Science Foundations of China (No. 61001039 and 60501004), and also supported by the Research Fund for the Doctoral Program of Higher Education of China (20090201120030).

REFERENCES

[1] K. S. Yee, "Numerical Solution of Initial Boundary Value Problems Involving Maxwell's Equations in Isotropic Media,"

IEEE Trans. Antennas Propagat., vol. 14, pp. 302-307, May 1966.

[2] D. T. Prescott and N. V. Shuley, "A Method for Incorporating Different Sized Cells Into the Finite-Difference Time-Domain Analysis Technique," *IEEE Microwave Guided Wave Lett.*, vol. 2, pp. 434-436, Nov. 1992.

[3] M. W. Chevalier, R. J. Luebbers, and V. P. Cable, "FDTD Local Grid with Material Traverse," *IEEE Trans. Antennas Propagat*, vol. 45, pp. 411-421, Mar. 1997.

[4] M. Okoniewski, E. Okoniewska, and M. A. Stuchly, "Three-Dimensional Subgridding Algorithm for FDTD," *IEEE Trans. Antennas Propagat.*, vol. 45, pp. 422-429, Mar. 1997.

[5] I. Ahmed and Z. Chen, "A Hybrid ADI-FDTD Subgridding Scheme for Efficient Electromagnetic Computation," *International Journal of Numerical Modeling, Electronic networks, devices and fields*, vol. 17, pp. 237-249, Jan. 2004.

[6] A. Monorchio and R. Mittra, "Time-Domain (FE/FDTD) Technique for Solving Complex Electromagnetic Problems," *IEEEE Microwave Guided Wave Lett*., vol. 8, pp. 93-95, Feb. 1998.

[7] S. Wang, "Numerical Examinations of the Stability of FDTD Subgridding Schemes," *The Applied Computational Electromagnetics Society (ACES) Journal,* vol. 22, pp. 189-194, 2007.

[8] J. Chen and J. Wang, "A 3-D Hybrid Implicit-Explicit FDTD Scheme with Weakly Conditional Stability," *Microwave Opt. Technol. Lett.*, vol. 48, pp. 2291-2294, Nov. 2006.

[9] J. Chen and J. Wang, "Comparison between HIE-FDTD Method and ADI-FDTD Method," *Microwave Opt. Technol. Lett.,* vol. 49, pp. 1001-1005, May 2007.

[10] J. Chen and J. Wang, "A Three-Dimensional Semi-Implicit FDTD Scheme for Calculation of Shielding Effectiveness of Enclosure with Thin Slots," *IEEE Trans. Electromagn. Compat.*, vol. 49, pp. 419-426, Feb. 2007.

[11] I. Ahmed and E. Li, "Conventional Perfectly Matched Layer for Weakly Conditionally Stable Hybrid Implicit and Explicit-FDTD Method," *Microwave Opt. Technol. Lett.,* vol. 49, pp. 3106-3109, Dec. 2007.

[12] J. Chen and J. Wang, "Numerical Simulation using HIE–FDTD Method to Estimate Various Antennas with Fine Scale Structures," *IEEE Trans. Antennas Propagat.*, vol. 55, pp. 3603-3612, Dec. 2007.